PROCEEDINGS A

rspa.royalsocietypublishing.org

Research

Article submitted to journal

Subject Areas:
Computer modelling and simulation, fluid mechanics, applied mathematics

Keywords:
Viscous froth model, physics of bubbles, foam rheology

Author for correspondence:
P. Grassia
e-mail: paul.grassia@strath.ac.uk

THE ROYAL SOCIETY
PUBLISHING

Viscous froth model applied to the dynamic simulation of bubbles flowing in a channel: Three-bubble case

C. Torres-Ulloa[1] and P. Grassia[1]

[1]Department of Chemical & Process Engineering, University of Strathclyde, James Weir Building, 75 Montrose St, Glasgow G1 1XJ, UK.

A two-dimensional foam system comprised of three bubbles is studied via simulations with the viscous froth model. Bubbles are arranged in a so called staircase configuration and move along a channel due to imposed driving back pressure. This flowing three-bubble system has been studied previously on the basis that it interpolates between a simpler staircase structure (a simple lens, which breaks up via so called topological transformations if driven at high pressure) and an infinite staircase (which sustains arbitrarily large driving pressure without breaking). Depending on bubble size relative to channel size, different solution branches for the three-bubble system were found: certain branches terminate (as for the simple lens) in topological transformations and others reach (as for an infinite staircase) a geometrically invariant migrating state. The methodology used previously was however a purely steady state one, and hence did not interrogate stability of the various branches, nor the role of imposing different driving pressures upon topological transformation type. To address this, unsteady state three-bubble simulations are realized here. Stable solution branches without topological transformation exist for comparatively low driving pressures. For sufficiently high imposed back pressures however, topological transformations occur, albeit with imposed pressure now influencing the transformation type.

1. Introduction

The study of microscale flows of multiphase systems including microbubbles or liquid foams has applications in processes involving drug manufacture, medical treatments,

minerals processing, material formation, and in the food and cosmetic industries [1–3]. In foam microfluidic applications in which bubbles flow through a confined geometry, including processes like enhanced oil recovery (EOR) [4], soil remediation [5], and foam sclerotherapy [6], the foam is used as a driving fluid to sweep a specific material, colloid pollutant or particles from the medium [7–9]. Due to foam's low mobility, by controlling how it moves, the flow of other fluids within the medium can be controlled also. How foam moves and rearranges inside a channel along which it is being transported is then a matter of great interest since the microscale dynamics impact the global process behaviour [10].

The rheology of such systems is complex. Liquid foams (which consist of dispersed gas trapped inside a liquid phase with energy tied to the gas-liquid interface) are themselves non-Newtonian fluids [11]. Depending on the relative amounts of liquid and gas (i.e. the liquid fraction), foam configurations will vary from a bubbly dispersion (wet foams), to packing in polyhedral cells (dry foams) [12]. In the latter scenario (the dry limit which we consider here), static foams try to find an equilibrium state in which bubbles fill space with their shapes being determined via total surface area minimization [13]. These systems can behave as solid-like or liquid-like, depending on the imposed shear stress. If the imposed stress is larger than a yield stress, the system will be set into motion. As the foam moves, certain liquid interfaces or bubble films are stretched, while others shrink until disappearing, eventually leading to rearrangements of the structure, with bubbles exchanging neighbours [14]. These rearrangements are the so called $T1$ topological transformations, and their order of occurrence is not always easy to predict a priori since different transformations may compete with one another, and in addition one transformation may trigger an avalanche of others occurring shortly afterwards [15–17].

The rate at which topological transformations are induced in a flowing foam depends on how rapidly the foam is sheared [18]. However foam also relaxes after each topological transformation, and the rate at which such relaxation occurs is inherent to the foam itself rather than how rapidly it is sheared [18]. This means that for a flowing foam, we make a distinction between slow flow (in which deformation of the foam is punctuated with intermittent topological transformations and their subsequent relaxations) and fast flow (in which $T1$ topological transformations are induced at a rate comparable with the relaxation rate post-$T1$) [19]. In the intermittent (i.e. slow-flowing) case it is not strictly necessary to resolve the relaxation process itself: on the scale of the slow imposed deformation, the relaxation is so fast that it appears to be instantaneous. In the fast-flowing case however this relaxation must be resolved, occurring as it does at a rate comparable with the rate at which the $T1$ transformations are induced by imposed deformation in the first place [19]. In addition to the bubble rearrangements (i.e. the aforementioned $T1$s), the dynamics of a foam flowing along a channel is affected by the foam structure/bubble configuration, volume of the bubbles, and the geometry of the channel of transport. All of these factors combined make the bubble-scale system behaviour difficult to predict [20].

Modelling foam motion on the bubble scale within fully three-dimensional systems can be computationally expensive. In microfluidic devices however, a two-dimensional foam system (see also section S 1 in supplementary material) is often considered, where we often just have a monolayer of bubbles across the depth of a microfluidic channel, albeit possibly with several bubbles stacked across the channel width and length. Indeed a typical geometry is a Hele-Shaw cell [14] in which a foam monolayer is confined between two glass plates with a small separation between them. In this configuration, film lengths along the plates are comparatively large relative to plate separation [21]. Films within a foam monolayer therefore appear as one-dimensional curves of negligible thickness when seen from above the top plate (see Figure 1), which is how models typically treat them [21]. The film endpoints are either on sidewalls of the Hele-Shaw cell (which when viewed from above the top plate appear to be upper and lower channel walls, and will be referred to in what follows as such) or at vertices away from those walls (with three films meeting at each vertex).

The purpose of the present work is to tackle some open questions (described in more detail in section 2) in the modelling of microfluidic and/or Hele-Shaw foam flows, having important implications for how foam bubbles arrange within a channel as they flow. Typically how bubbles

arrange depends on bubble size relative to channel size. Here however issues mentioned above such as imposed stress (or more generally imposed pressure driving the flow along), rate dependency (slow versus fast flow) and $T1$ topological transformations will all turn out to be central to the discussion. Via simulations of foam flows, insights will be gained in particular into how systems behave when different types of $T1$ compete: in such cases, it will turn out that the type of $T1$ selected and thereby the bubble arrangement can become sensitive to driving pressure even for a specified set of bubble sizes. Moreover, even though high driving pressures associated with fast flows are conventionally thought of as inducing $T1$s, one of the most interesting predictions of the simulations will turn out to be that under certain circumstances high driving pressures actually prevent $T1$s. By and large though, increasing driving pressure tends to cause $T1$s, rather than preventing them. Increasing pressure in this fashion also typically causes the system to break via $T1$ in less time and with less distance travelled along the channel. As a result, for a channel of a specified finite length, it is typically possible to find a certain particular pressure at which the structure can be driven along the channel as quickly as possible without breaking. Moreover the shorter the channel, typically the faster the structure can be driven and still avoid breaking.

The rest of this work is laid out as follows. Section 2 reviews what is already known about modelling bubbles flowing in Hele-Shaw cells, introduces the three-bubble system and the different types of topological transformations it might reach and, as already mentioned, identifies the specific open questions that the present work will address. In section 3, we summarize the simulation methodology to be employed. Results are given in section 4. Finally in section 5 we offer conclusions. Additional analysis and results are relegated to supplementary material.

2. Context and open questions

This section reviews the context leading up to the particular system that we choose to study, which consists of three bubbles (see e.g. Figure 1(c)) moving along a channel in a Hele-Shaw cell. Background information is given explaining why the three-bubble case turns out to be of such interest, and what the open questions are that we can address by modelling it.

The present section is laid out as follows. Section 2(a) reviews the physical model to be employed, whereas section 2(b) describes the rate-dependent flow behaviours that the model predicts. Section 2(c) then considers two distinct systems, one that exhibits rate dependency leading to topological transformations and another that does not. After that section 2(d) introduces the specific system to be studied here (namely the three-bubble system) and indicates how it interpolates between the cases that are already discussed in section 2(c). Finally information about the possible behaviours of the three-bubble system and open questions to be addressed here about those behaviours are discussed in sections 2(e)–2(f).

(a) Viscous froth model

In the introduction it was already mentioned that differences can occur between slow-flowing foam and fast-flowing foam. To understand those differences, we need a model that can distinguish between slow-flowing and fast-flowing states. The model of choice here is the so called viscous froth model [11, 21–23]. This model (as described in more detail in supplementary material section S 1(a)) considers the forces upon foam films, namely bubble pressure effects and capillary (surface tension/curvature) effects, equating any mismatch between them to a viscous drag force [24], with the viscous drag here being associated with moving films relative to the plates of the confining Hele-Shaw cell. In particular, viscous drag forces govern how rapidly foam relaxes after a $T1$ transformation, so that the viscous froth model (unlike a number of models employed in other studies [16,25–28]) is by its nature able to resolve such relaxation processes. In the interests of simplicity, a linear relation between drag and velocity will be assumed here. Balancing the various forces then defines a characteristic relaxation velocity and hence the aforementioned characteristic relaxation rate. However if an external driving pressure is imposed, over and above the original equilibrium bubble pressures that apply within a static system, the viscous froth model can predict foam films propagating at a migration velocity

very different from the characteristic relaxation velocity. By explicitly incorporating the relaxation processes present in a foam moving through a Hele-Shaw cell, the viscous froth model therefore has the properties we require, namely it manages to describe rate-dependent effects in fast flows [29–32] that slow-flowing foam models would fail to capture.

(b) Rate-dependent flow behaviours and topological transformations

Having now identified a rate-dependent model, it is possible to use it to explore the link between rate-dependent flow behaviours and $T1$ topological transformations. In particular in [1] and in [11], the viscous froth model was applied to a train of bubbles arranged in a staircase structure (see e.g. the configuration in Figure 1(a)), but flowing now through a U-bend channel (unlike Figure 1(a) which specifically shows a straight channel). By imposing different back pressures to drive the system, it could be set into motion at different migration velocities relative to the channel walls [33]. From [11] it was observed that for low velocities, there was no $T1$ topological transformation in such a system. However, for a sufficiently high velocity (or equivalently for a sufficiently high imposed back pressure driving the flow), the structure exhibited a $T1$ transformation, with the bubbles on the inner side of the bend tending to overtake those on the outer side. Experimental work in [1] using the U-bend geometry was found to support the viscous froth model predictions.

The physical mechanism for producing $T1$ transformations in such a system is as follows. To maintain their relative position, points on the outside of the bend need to move faster than points on the inside of the bend. As a result points on the outside incur more viscous drag, such that that drag is asymmetric across the channel: what asymmetric means in this context is simply that points on the outside of the bend have more drag than those on the inside, due to the faster motion towards the outside. As the overall migration velocity increases (due to an increasing imposed driving pressure), the asymmetry in the drag forces becomes greater, and eventually the system's internal relaxation rate becomes insufficient to compensate for it. Bubbles on the outside then fall behind those on the inside (or equivalently those on the inside overtake those on the outside) and eventually a topological transformation occurs: beyond a critical imposed driving pressure therefore, bubbles exchange neighbours. As demonstrated by [1] then, rate dependency significantly affects foam flows in Hele-Shaw cell systems. However it is essential to have rate dependency coupled to asymmetry (specifically the asymmetry between the parts of the staircase on the inside of the bend and on the outside of the bend), so as to lead to drag forces on a moving system that are able to break the structure apart.

This then raises an interesting question. If $T1$s are associated with asymmetry, then in principle they can still occur even in a straight channel if asymmetry is present for some other reason. The simplest way to achieve this is to have an odd number N of bubbles arranged in a staircase, so that one side of the staircase has more films (and hence when moving, more drag on those films) than the other. In order to capture that asymmetry effect in a very simple system, the work of [14] therefore considered a drastically truncated staircase, i.e. the case $N = 1$ (see Figure 1(b)). This consisted of just one bubble on one of the channel walls, with an additional film attaching the bubble to the opposite channel wall. Plateau's laws govern the angles at which films meet one another and meet channel walls: see the caption of Figure 1 for details. This system was called a viscous froth lens or simple lens, and its behaviour is described next.

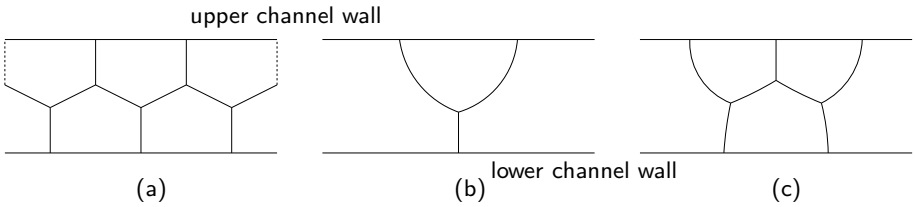

Figure 1: Foam structures in a confined straight channel, looking down at a Hele-Shaw cell from above, so the upper and lower channel walls are in fact sidewalls of the original Hele-Shaw cell. Bubble films obey Plateau's laws: they connect three by three in vertices, subtending an angle of 120° (or $2\pi/3$) and meeting the cell's boundaries forming an angle of 90° (or $\pi/2$), even when the foam is set into motion [14]. (a) Infinite staircase. (b) Simple lens. (c) Three-bubble system. The simple lens is a drastically truncated version of the infinite staircase, whereas the three-bubble case interpolates between those two systems.

(c) Simple lens system contrasted with infinite staircase

When the simple lens system was studied via the viscous froth model it was observed by [14] that for low imposed back pressures there is no topological transformation, but as the driving pressure is increased, a topological transformation occurs. What then happens is that the bubble in Figure 1(b) is overtaken by the film originally attached to it, and eventually that film detaches and leaves the bubble behind. However the driving pressure at which the topological transformation occurs turns out to be sensitive to bubble size, i.e. to bubble area in a two-dimensional view like that in Figure 1(b), implying that bubble size is also a relevant variable to study. In [14], it was demonstrated that small bubble areas exhibit more resistance to break up than big bubbles do (sizes being measured here relative to the channel of transport). Small bubbles are of course enclosed by short films, and so the drag force associated with those films when they move is rather limited. This then limits any asymmetry of the drag in spite of having two films on one side of the channel but only a single film on the other. As already mentioned, topological transformations rely on coupling between rapid motion and asymmetry. By limiting asymmetry, small bubbles resist transformation out to higher driving pressure (i.e. higher velocity). Larger bubbles on the other hand have longer films, more asymmetry in the drag, and hence more susceptibility to break via topological transformations.

It is then interesting to contrast the simple lens with a much more symmetric system, namely the infinite staircase structure (Figure 1(a)). Provided flow occurs along a straight channel, bubbles in the infinite staircase are found to maintain their relative position with respect to their neighbours, even when high imposed back pressures are applied [15]. Indeed for the viscous froth model, the infinite staircase in a straight channel corresponds to a geometrically invariant state. Under any imposed driving pressure no matter how large, bubbles can move without deforming their shape, such that no $T1$ transformations would ever occur. For N-bubble systems, there is a therefore a significant difference in behaviour between the simple lens $N=1$ and the infinite staircase $N\to\infty$. It was to elucidate these distinct behaviours and find a system that might somehow form a bridge between them, that a recent study of [34] elected to study the three-bubble system $N=3$ (see Figure 1(c)). The outcomes of that study are described next.

(d) Three-bubble system

The three-bubble system (shown in Figure 1(c) and in more detail in Figure 2) represents a step forward in complexity compared to the simple lens. The study of [34] considered three bubbles ($\mathcal{B}_1$, $\mathcal{B}_2$ and $\mathcal{B}_3$) of various sizes relative to the channel size and also of various sizes relative to each other. As section S 2 in supplementary material describes in much more detail, bubble size is determined here by the bubble areas A_1, A_2, A_3 (for simplicity, it is assumed that $A_1=A_3$, although A_2 might differ). Via the viscous froth model, steady state solutions were obtained for the system propagating steadily at some velocity v along a channel under the influence of an imposed back pressure p_b, this

pressure p_b itself being distinct from the individual bubble pressures p_1, p_2 and p_3. Starting from equilibrium with no back pressure (Figure 2(a)) and then gradually increasing the imposed back pressure, it was explored how the steadily propagating configuration evolved as the back pressure changed (Figure 2(b)), and thereby whether there might be certain critical pressures at which the structure would break up. The distribution of bubble areas turned out to affect not only the pressure required to break the structure but also the specific manner in which it broke, there being now several different ways in which breakage could occur (see Figure 3). Different types of break up were not seen in the simple lens case [14], which being much simpler geometrically than the three-bubble system could only ever break up in one way, i.e. a film detaching whilst leaving a bubble behind. An analogous mode of break up could occur for the three-bubble system [34], but it was by no means the exclusive break up mode.

Furthermore, for certain bubble area distributions, the three-bubble system was observed to reach a geometrically invariant state [34] (again see Figure 3). In such cases, the structure deforms geometrically and also moves faster as imposed back pressure increases, but never undergoes a $T1$. Instead, for high enough back pressure eventually a configuration is reached in which no further geometric deformation occurs, and instead increases in the pressure are simply absorbed by increases in the propagation velocity for an established geometry. This then is behaviour akin to the infinite staircase. The simple lens system, on the other hand, could not admit the aforementioned geometrically invariant state [14,34]: it is necessary to consider at least a three-bubble system in order for it to be seen at all.

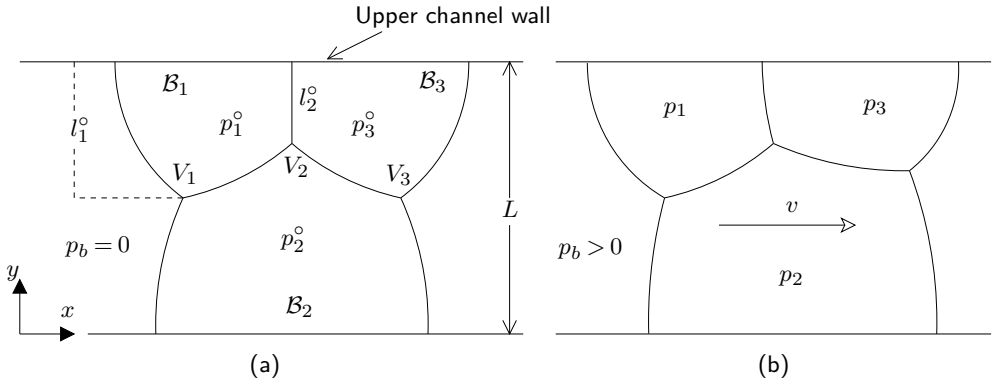

Figure 2: (a) Equilibrium system for a channel of dimensionless width $L = 1$. The pressures of bubbles $\mathcal{B}_1$, $\mathcal{B}_2$ and $\mathcal{B}_3$ are p_1°, p_2° and p_3° respectively, with the superscript "$\circ$" here denoting equilibrium. The imposed back pressure in this case is $p_b = 0$. Also in this case $p_1^\circ = p_3^\circ$ because bubbles $\mathcal{B}_1$ and $\mathcal{B}_3$ are assumed to have the same area. The distance between the upper channel wall and the vertex V_1 and V_3 is l_1°, and between the upper channel wall and the vertex V_2 is l_2°. The system is comprised of seven films j_{ij} connecting at the respective vertices. Every film forms an angle of $\pi/2$ with the respective wall of the channel and an angle $2\pi/3$ with other films. The lengths of the films in equilibrium are $\mathcal{L}_{01}^\circ = \mathcal{L}_{30}^\circ$, $\mathcal{L}_{23}^\circ = \mathcal{L}_{12}^\circ$ and $\mathcal{L}_{02}^\circ = \mathcal{L}_{20}^\circ$. Moreover $\mathcal{L}_{13}^\circ = l_2^\circ$. When two subscripts are shown here, they denote the bubbles which a given film separates. (b) The system is set in motion, travelling at a unknown migration velocity v, as a consequence of an imposed back pressure $p_b > 0$. Bubble pressures p_i and film lengths $\mathcal{L}_{ij}$ also change.

What is apparent from the foregoing discussion is that depending on the bubble areas selected, the three-bubble system can interpolate between behaviours of the simple lens and behaviours of the infinite staircase, as well as exhibiting some complex behaviours all of its own. In the discussion that follows (sections 2(e)–2(f)) we give further information about the possible behaviours that [34] identified for the three-bubble system, and well as some of the open questions about such behaviours.

(e) Behaviours of the three-bubble system

As mentioned, steady state solutions of the three-bubble system have already been obtained for a wide range of initial bubble area distributions and a wide range of driving pressures [34]. As is apparent from Figure 1(c) and also from Figure 2, the system consists of two bubbles adjacent to an upper channel wall plus one bubble adjacent to a lower channel wall, with seven films which join threefold at three separate vertices. As section S 2(a) in supplementary material explains in more detail, the film separating bubbles $\mathcal{B}_i$ and $\mathcal{B}_j$ is denoted $\jmath_{ij}$ and has length $\mathcal{L}_{ij}$. If a subscript within $\jmath_{ij}$ or $\mathcal{L}_{ij}$ is zero, it indicates a film on the outside of the structure. Vertices are labelled V_1, V_2 and V_3 (see Figure 2).

In the equilibrium state (Figure 2(a)), the distance between V_1 or V_3 and the upper channel wall is denoted l_1° (the superscript here denotes equilibrium). Meanwhile the distance between V_2 and the upper channel wall is denoted l_2°. It is convenient to work in a dimensionless system in which the distance between the upper and lower channel walls is unity, implying then that $l_2^\circ < l_1^\circ < 1$. As section S 2 in supplementary material explains, these distances l_1° and l_2° (see Figure 2) are useful surrogates for bubble areas, since by fixing them we fix the bubble areas [34].

The work of [34] then proceeded to increase the imposed back pressure p_b to shift the system out of equilibrium. Any pressure increases however necessarily occurred slowly i.e. quasistatically, because the intention was to maintain the system at steady state, even though out of equilibrium. Depending on the bubble areas selected (or equivalently depending on l_1° and l_2°), it was shown by [34] that increasing the imposed back pressure p_b in this quasistatic fashion could lead to different possible outcomes. Specifically the three-bubble system can undergo an internal vertex-vertex collision away from any wall denoted $T1_c$, or a $T1$ at the upper channel wall $T1_u$ (analogous to what happens for a simple lens [14]), or a $T1$ at the lower channel wall $T1_l$. Variants of the $T1_u$ and $T1_l$ can also occur, respectively denoted $T1_{u'}$ and $T1_{l'}$. Details of exactly what these transformations involve are indicated in Figure 3 and further discussed in supplementary material section S 2(b). All the transformations involve a film shrinking to zero length. However, for each different transformation, a different film is involved.

In addition to having different types of $T1$, there are also conceptually two different ways in which each of these transformations can take place, again depending on the bubble area distribution of the system [34]. The first way is that as the driving back pressure is gradually increased, certain films grow, whilst others gradually shrink, the system passing through a sequence of steadily migrating states until eventually (when a certain critical pressure denoted p_b^* is reached) one of the shrinking films attains zero length, leading directly to one of the $T1$ transformations mentioned earlier. In this fashion the topological transformation is itself attained quasistatically matching the quasistatic changes in pressure. Therefore, prior to the $T1$ happening, the film that eventually shrinks to zero length can be maintained arbitrarily short for an arbitrarily long time, provided changes in driving pressure are sufficiently slow. The second way in which a transformation can be reached is that as driving pressure is gradually increased, again certain films grow, whilst others shrink, the system passing through a sequence of steady states until eventually (when a certain pressure again denoted p_b^* is reached) the steady solution branch comes to an end, and steady solutions thereafter cease to exist, even though all films still have finite length. The system must then run away to a topological transformation (with a particular film length then vanishing) but this happens dynamically rather than via a sequence of steady states. The rate of any subsequent evolution is then determined by the internal dynamics of the system itself [14], rather than the rate at which an externally imposed pressure is changed.

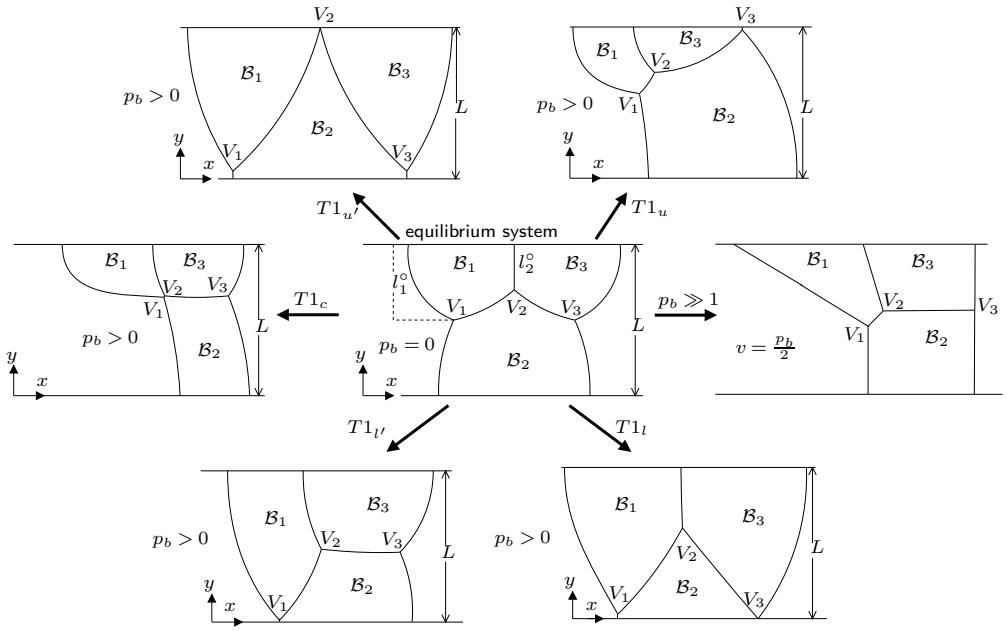

Figure 3: In the middle of this figure we show the three-bubble equilibrium structure (bubbles $\mathcal{B}_1$, $\mathcal{B}_2$ and $\mathcal{B}_3$ and vertices V_1, V_2 and V_3) in a channel of dimensionless width $L = 1$. A back pressure p_b is then imposed to drive the system out of equilibrium. Each possible outcome, obtained for a sufficiently high imposed back pressure, is shown around the periphery: topological transformations $T1_{u'}$ (film length $\mathcal{L}_{13}$ of the film separating bubbles $\mathcal{B}_1$ and $\mathcal{B}_3$ vanishes) and $T1_u$ ($\mathcal{L}_{30}$ vanishes) correspond to a vertex reaching the upper channel wall; $T1_c$ corresponds to vertex-vertex collision ($\mathcal{L}_{12}$ vanishes); $T1_{l'}$ ($\mathcal{L}_{02}$ vanishes) and $T1_l$ ($\mathcal{L}_{20}$ vanishes) correspond to a vertex reaching the lower channel wall. In the case labelled $p_b \gg 1$ there is no $T1$, but instead a geometrically invariant state is reached.

Mathematically this second scenario is associated with the original steady solution branch meeting a second steady solution branch in what is called a saddle-node bifurcation. What the saddle-node bifurcation involves specifically will be discussed in more detail later. Physically however it can be thought of as the $T1$ being preempted [35,36]. In other words, it is no longer possible to attain very short film lengths gradually, nor to maintain very short film lengths indefinitely. Instead there is a certain finite film length below which it becomes inevitable that the system runs away to $T1$, and the film in question shrinks and disappears. The work of [35,36] is however different from what we study here. The system of [35,36] was kept at equilibrium up to a saddle-node bifurcation, with $T1$s induced by shifting system boundaries. Here however the system is steadily propagating (but out of equilibrium) up to the saddle-node bifurcation: $T1$ is induced by changing imposing driving pressure, thereby shifting the system further and further away from equilibrium.

Whilst the saddle-node scenario was ubiquitous for the simple lens (see supplementary material section S 3 for details), in the three-bubble system studied by [34], the quasistatic type of $T1$ happened in most cases, whereas the saddle-node type $T1$ was the exception rather than the rule. In the three-bubble system, saddle-node cases tended to be confined within "buffer regions" where two or more different types of $T1$ (i.e. $T1_c$, $T1_u$ or $T1_l$ along with variants $T1_{u'}$ and $T1_{l'}$ as shown in Figure 3) were competing with each other (see sections S 2(b) and S 4 in supplementary material for details). It is precisely because of the above mentioned competition that these saddle-node buffer regions are likely to be interesting to study in more detail, since the different modes of $T1$ could compete to be selected depending how the system is driven. This notion is discussed further below, with a highlight on open questions.

(f) Open questions for the three-bubble system

It is actually possible to continue tracking steady solutions around a saddle-node bifurcation onto a second branch, but what then happens is that driving pressure tends to decrease rather than increase [34]. The second branch eventually reaches a topological transformation at some driving pressure $p_{b,T1}$ which is lower than the pressure p_b^* at which the bifurcation appeared. However whether it is even meaningful to track the branch in this fashion is unclear, since the branch could be dynamically unstable. The methodology used by [34] only tracks steady solution branches, but does not interrogate their stability. Determining which one of the aforementioned solution branches is stable is therefore one of the open questions of the present work.

The methodology of [34] was, as has been mentioned, a steady state one (i.e. it involves passing through sequences of steady states via slow increases in driving pressure until $T1$ occurs). Details of what the steady state approach predicts are discussed in section S 4 in supplementary material. However, a more likely scenario in experiment is that, starting from an equilibrium (i.e. static) state, a sudden step in driving pressure would be imposed. How the system responds is then an inherently dynamic question, not a steady state one. Indeed there is no guarantee that the same state is reached for a sudden step increase in pressure as opposed to a gradual increase. This then is another open question to be addressed. The critical pressure needed to break a system dynamically (denoted p_b^{**} say) might well differ from the critical pressure p_b^* needed to break it via the steady state approach (see e.g. section 4(c) and also section S 7 in supplementary material). Moreover, the domain of imposed pressures available to the dynamical simulation is far wider than the domain available to the steady state computation. In the steady state case, the slow increase in pressure would stop as soon as the structure breaks via topological transformation. For a dynamic simulation by contrast, the system can be driven immediately with a pressure well in excess of the minimum pressure needed to break it. The way in which the system breaks might then depend on the particular pressure imposed, which again is an open question.

As alluded to already, an alternative situation found by [34] depending again on bubble sizes, is to have no $T1$ whatsoever (see also Figure 3). The system instead reaches, in the limit of large imposed back pressure a geometrically invariant state, which does not suffer any further deformation as the imposed pressure continues to increase, but instead merely moves faster and faster (see [15] for systems exhibiting similar behaviour). For the three-bubble system, this geometrically invariant state turned out only to occur for a relatively limited set of bubble areas (see phase diagram in the supplementary material Figure S 2). However it does underline that the three-bubble system can admit behaviours akin to the infinite staircase, and hence indeed interpolates between the simple lens and the infinite staircase as we have claimed. One of the findings from [34] was that a necessary condition (in terms of bubble sizes) could be formulated for existence of a geometrically invariant state. However only a small subset of the states satisfying the necessary condition actually attained the geometrically invariant state, the rest undergoing $T1$ instead. Remember however, as has been explained, the work of [34] involved gradual increases in driving pressure. A sudden imposition of a driving pressure rather than a gradual increase might make the geometrically invariant state more prevalent or less so. This then is yet another open question to be addressed.

In order to address the various open questions alluded to above, in this work we study the three-bubble system by evolving it dynamically from the equilibrium state, up the point where the system undergoes a topological transformations or else attains a geometrically invariant state. As we will see, the dynamic approach employed here does not always match up with the steady state approach used by [34], particularly when different types of $T1$ are competing.

3. Unsteady state simulation methodology

In this section we summarize the methodology used to perform unsteady state simulations, which is based, as already mentioned, on the work in [14]. Further details are available in section S 5 in the supplementary material. Here we start in section 3(a) by introducing the viscous froth model equation (details in section S 1(a) in supplementary material), which is used to capture the system

evolution. Then in section 3(b) we define the spatial discretization and time evolution. Finally in section 3(c) we specify the condition under which a steadily propagating structure is considered to be achieved.

(a) Equation governing film motion

Equation (S 1.1), as given in supplementary material section S 1(a), corresponds to the dimensional form of the viscous froth model, with a linear viscous drag law [24]. A rescaled version of the model can be deduced, as obtained in [14], so that the viscous froth model can be written in its dimensionless form as

$$v_\perp = \Delta p - \kappa \tag{3.1}$$

which is the form we use here, with $v_\perp$ being normal velocity of a film element, Δp being pressure difference across a film, and κ being film curvature, all in dimensionless form. Here the left-hand side of the equation (3.1) represents the linear viscous drag force, and the right-hand side represents the driving forces, which can only be in balance for a static film (following Laplace's law) at equilibrium, but not for a system moving steadily relative to channel of transport. Note that equation (3.1) specifies normal motion but not tangential motion: this is on the basis that tangential motion does not directly impact film shapes (see section S 1(a) for further discussion).

(b) Discretization and time evolution

Once the equilibrium structure is set by fixing l_1° and l_2° (with $l_2^\circ < l_1^\circ < 1$ since distance between the upper and lower channel walls is unity in the dimensionless system), each film $\jmath_{ij}$ is discretized into a finite number of points, depending on the film's length $\mathcal{L}_{ij}^\circ$ at equilibrium (see section S 5(a) in supplementary material). In our dimensionless system (with unit width across the channel), film segment lengths are chosen so as to ensure that each film is comprised of a least five points (again see section S 5(a) in supplementary material; the reason for requiring at least five points per film is described in section S 5(c) and is also alluded to below). If a film length happens to be shorter than a minimum allowed length (chosen here to be 0.002, see section S 5(a)) a topological transformation is carried out on the system. Otherwise, for a given imposed back pressure p_b, each film point moves over time, discretized in steps of δt.

Motion (see section S 5(b) in supplementary material) is in the normal direction $\mathbf{n}$ with a velocity $v_\perp$ equal to the difference between the pressure change across the film Δp, and the film curvature κ (see sections S 5(c)–S 5(d) in supplementary material), which is what the viscous froth model captures (see equation (3.1) and also section S 5(b) in the supplementary material). Here the chosen time step δt is sensitive to the spatial discretization. Hence the smaller is the allowed separation between points, the smaller the time step has to be (see section S 5(b) in the supplementary material for details). The time step here can take values of $\delta t \in [10^{-7}, 10^{-5}]$ [37]. On the other hand, as specified in section S 5(c) in the supplementary material, curvature κ is computed numerically, in such a fashion so as to ensure second order accuracy in space (this is incidentally what requires at least five points per film). Bubble pressures are computed at each time step aiming to keep bubble areas invariant as specified in section S 5(d) in the supplementary material. After each time step, the area constraints might still be violated by very small amounts (owing to truncation error in the numerical scheme). These constraint violations can however be corrected by following [11] (see section S 5(e) in the supplementary material for details). Moreover, at each time step we also have to compute positions of vertices for which we use the solution for a Steiner point, as explained in section S 5(f) in the supplementary material. To retain second order accuracy, we also implement a regridding algorithm, as specified in section S 5(g) in the supplementary material.

(c) Conditions to reach steady state

As we suddenly impose an arbitrary back pressure p_b upon the system, it will be set into motion. The films then undergo deformation and bubble shapes change. If p_b is smaller than the aforementioned

critical value p_b^{**} required to induce a topological transformation, a steady state migrating structure should eventually be attained. In this steadily migrating structure, bubble shapes are no longer changing with time and film lengths remain constant.

A criterion is needed to determine whether the system has reached a steadily migrating shape. As established in the numerical method, this is based on the system's energy measured at each time step. Energy in this context is the sum total of all film lengths. If the energy varies sufficiently slowly over time $|\mathrm{d}E/\mathrm{d}t| < 10^{-5}$ for at least one dimensionless time unit (see section S 1(a) in supplementary material for what this represents in dimensional time), steady state is assumed to have been reached.

4. Unsteady state results

In this section we present unsteady state simulation results, obtained for a wide domain of bubble sizes, specifically for values of $l_1^\circ \in [0.1, 0.2, ..., 0.9, 0.96]$, with values of $l_2^\circ/l_1^\circ \in [0.1, 0.2, ..., 0.9]$. The rationale for selecting $l_1^\circ = 0.96$ in particular was to allow exploration of $T1_l$ transformations: the steady state analysis [34] (see also section S 4) suggests that such transformations only tend to occur with very large l_1° values. As l_1° reduces to 0.9 or less, $T1_c$, $T1_u$ and $T1_{l'}$ transformations occur instead. Note that the present work only follows systems up to their first topological transformation. The methodology of section 3 can actually track systems through multiple topological transformations, but here we restrict consideration just to the first of them. Note moreover that the $T1_{u'}$ is not considered here. Having a $T1_{u'}$ as the first topological transformation turns out to be very rare (as [34] explained) and in fact none of the states in the domain to be explored here break initially via a $T1_{u'}$.

We start in section 4(a) by comparing a steadily migrating system obtained via steady state solution in [34], with the time evolution of a system obtained via unsteady state simulation here: this benchmarks our approach. Then in section 4(b) we determine which one of two possible steady solution branches, as found in [34], is the stable one. In section 4(c) we compute the time and distance travelled for different systems starting from equilibrium up to them reaching their first topological transformation. These computations are done for various imposed back pressures p_b. Examples are found in which the pressure needed to break the system dynamically differs from the pressure needed to break it via a steady state approach. Remarkably systems are also found which do not break at all when driven dynamically by suddenly imposing a large pressure, but which would certainly break if the same pressure were to be attained gradually as the steady state approach of [34] would envisage. In addition, it is shown how the type of topological transformation that a given system undergoes can change according to the imposed back pressure: all this is studied in section 4(d).

Additional results are presented within section S 6 in supplementary material. Section S 6(a) verifies that it is possible to find systems that admit steady states which exist only at large pressures but not necessarily at lower pressures: this then helps to explain some of the findings in section 4(c). Section S 6(b) provides further details of a system undergoing $T1$ at pressures lower than expected by the steady state approach, so as to complement the results in section 4(c). Section S 6(c) gives more details of dynamic stability of various branches, to complement the results in section 4(b). After that section S 6(d) gives a further discussion of systems that transition between selecting different $T1$ types according to the pressure imposed upon them, complementing some of the results of sections 4(c)–4(d). Section S 6(e) looks at statistics of the three-bubble system $T1$ behaviours to establish which are common and which are less common, particularly as imposed back pressures are changed. Section S 6(f) compares the three-bubble system and the simple lens. An analogous comparison was already considered by [34], but in the present work dynamical behaviour, not steady state behaviour, is analysed.

(a) Approach to the steady state

Here we compare a steadily migrating structure obtained via unsteady state simulation after a sufficient elapsed time, with a structure obtained for the same system (with the same bubble areas) but via steady state solution. This is what Figure 4 shows, starting with a system set up at equilibrium

with $l_1^\circ = 0.5$ and $l_2^\circ/l_1^\circ = 0.5$. In Figure 4(a) we find that, for the same imposed back pressure $p_b = 10$, the unsteady state simulation eventually superposes the steady state solution. Any residual difference between the two structures at longer times is a consequence of truncation error in the unsteady state numerical scheme, this scheme being computed on a specified grid (see section S 5(a)). The steady state solution is not tied to a particular grid however (see section S 2(a)).

In Figure 4(b) we can see that the energy E (i.e. the sum of all the film lengths, which is conveniently normalised here by the energy of initial equilibrium state E°) increases rapidly at early times. However as time proceeds $\mathrm{d}E/\mathrm{d}t$ decreases, i.e. the system deformation rate slows down over time. This is also reflected in Figure 4(a), where at time $t = 0.5$ we see that the structure shows a noticeable difference from the equilibrium system, however, after that time, changes in the configuration towards the steady state are much more gradual. By time $t \approx 2.87$, the value of $\mathrm{d}E/\mathrm{d}t$ is small enough that our criterion for reaching steady state is attained (see section 3(c)), and in Figure 4(a) the unsteady state solution effectively overlays the steady state one.

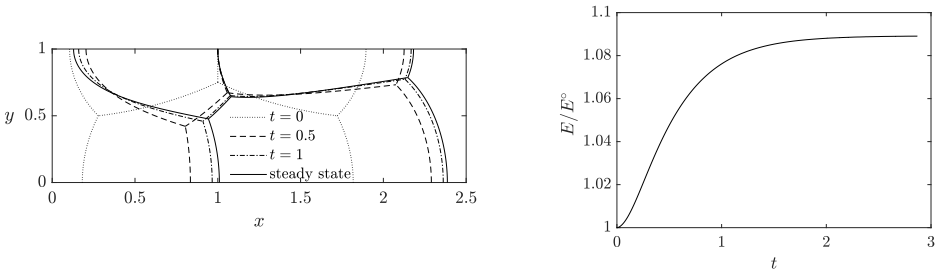

(a) (b)

Figure 4: (a) Comparison between the steady state solution and the unsteady state simulation for a structure with $l_1^\circ = 0.5$ and $l_2^\circ/l_1^\circ = 0.5$ in the equilibrium. In each case the solution is obtained for an imposed back pressure $p_b = 10$. For the unsteady state we started from an equilibrium state and then suddenly increased the back pressure from $p_b = 0$ to $p_b = 10$. Then at time $t \approx 2.87$ the system has reached steady state, according to the criterion established here. (b) Energy E normalised by equilibrium energy E° as a function of time t. Energy in this context is just the sum of the film lengths.

(b) Determining the stable solution branch

As has been mentioned in section 2(e) (see also section S 3), by obtaining steady state solutions it was found by [34] that some three-bubble systems might reach a saddle-node bifurcation point, at which two different solution branches were proven to exist (see Figure 5(b) later on for an illustration). The first branch connected the equilibrium state (at p_b identically zero) to a saddle-node bifurcation point at some $p_b = p_b^*$. The second branch which had higher energy than the first, turned out to connect the saddle-node bifurcation point to a $T1$ topological transformation point at $p_b = p_{b,T1}$ with $p_{b,T1} < p_b^*$, meaning that p_b decreased moving along this branch. This same phenomenon was seen in the simple lens system [14], where the second solution branch was proven to be unstable. Based on [14], in [34] it was assumed that the second solution branch was the unstable one in the three-bubble system also, however a definitive demonstration of this was not given.

(i) Unsteady simulation starting from the second solution branch

Here, to explore stability of various solution branches, we perform an unsteady state simulation. We start now with a system not at equilibrium, but instead that is already propagating steadily, albeit on the second (higher energy) steady solution branch. On this higher energy solution branch p_b is decreasing as the system approaches a topological transformation (see Figure 5(b)). We select

a system which, had it been at equilibrium, would have $l_1^\circ = 0.5$ and $l_2^\circ/l_1^\circ = 0.41$, but is instead moving steadily as a result of an imposed back pressure $p_b = 7.801$. This is lower than $p_b^* \approx 7.87$ (the maximum imposed back pressure at the saddle-node bifurcation) but higher than $p_{b,T1} \approx 7.61$ (the back pressure at which the solution branch would undergo a topological transformation, specifically a $T1_u$ in this case).

The studied system is found to be in a buffer region in which, according to a steady state analysis, $T1_u$ is competing with $T1_c$ (see supplementary material section S 4(a) for details). For instance, if for the same $l_1^\circ = 0.5$, a value $l_2^\circ/l_1^\circ \leq 0.372$ is selected, the $T1_u$ is found on the first solution branch (with p_b increasing starting from equilibrium), i.e. the $T1_u$ is reached quasistatically rather than via a saddle-node bifurcation. On the other hand, if $0.432 \leq l_2^\circ/l_1^\circ \leq 0.491$ the system undergoes $T1_c$ (not $T1_u$) on the second solution branch (with p_b now decreasing on the approach to $T1$). For values of $l_2^\circ/l_1^\circ > 0.491$ the system undergoes $T1_c$ on the first solution branch (with p_b increasing).

Returning to the system of interest, the unsteady state simulation methodology now applies. As mentioned the initial condition is a steady solution on a second solution branch with $p_b = 7.801$ and the system is then discretized as explained in section 3(b). Then we impose a very slightly different back pressure $p_b = 7.8$ (at what is considered to be time $t = 0$), so the initial condition is close to the steady solution at $p_b = 7.8$, but not exactly the same: a slight perturbation has in effect been imposed. Then the system is evolved over time.

Three different scenarios are possible. A first scenario is that the system, whilst conserving its topology, migrates away from its current shape to a different state (the system energy increasing or decreasing, with some films shrinking and others stretching), eventually reaching a new steady state after a certain amount of time: the system might for instance migrate from the second steady solution branch to the first one. A second scenario is that the system migrates away from its current shape until it reaches a topological transformation. Both of these two scenarios imply that the chosen steady state solution branch is unstable. In a third scenario, the system would not undergo any significant change in bubble shape nor in total film energy, suggesting that the high energy steady state branch was (unexpectedly perhaps) stable.

(ii) Migration from one steady state to another

For the selected system, we obtain that this actually migrates away from the original structure given at time $t = 0$, eventually reaching a new steady state solution, i.e. the first of the above mentioned scenarios. This new steady state structure coincides with that obtained for the same pressure $p_b = 7.8$, but now on the first solution branch, thereby confirming that the first solution branch is the stable one. In Figure 5(a) we can see the steady state solution shape of the selected system on the second solution branch (dotted line in Figure 5(a), structure at time $t = 0$ in the unsteady state simulation), and also the steady state solution shape on the first solution branch (see solid line in Figure 5(a)). The bold dotted line in Figure 5(a) (more easily seen in the inset) corresponds to the final state obtained via unsteady state simulation (reached, according to our criterion for achieving steady state, at time $t \approx 7.23$): clearly this matches with the solid line. Figure 5(b) shows the system energy for the steady state solution against different imposed back pressures. Here we can see how via dynamic simulation the system set up at the given p_b using the steady state solution on the second solution branch (higher energy), migrates to a state on the first solution branch (lower energy) as time proceeds (again this is easier to see in the inset).

In section S 6(c)i in the supplementary material, we study the same system (same values of $l_1^\circ = 0.5$ and $l_2^\circ/l_1^\circ = 0.41$), but considering a wider range of starting points for p_b on the second steady state solution branch. In all the studied cases, even for values of p_b very close to p_b^*, and also values very close to $p_{b,T1}$, the system migrates to the first solution branch (of lower energy). To demonstrate moreover that the findings are not specific to just one set of l_1° and l_2°/l_1° values, an additional case was also studied in section S 6(c)i in the supplementary material, which consists of a system with $l_1^\circ = 0.9$ and $l_2^\circ/l_1^\circ = 0.3$ at equilibrium. For this system, a similar situation was observed: in each case the stable migrating structure corresponds to the first solution branch. In both studied

cases, we have found that the steady state system on a second solution branch migrates dynamically back to the first branch.

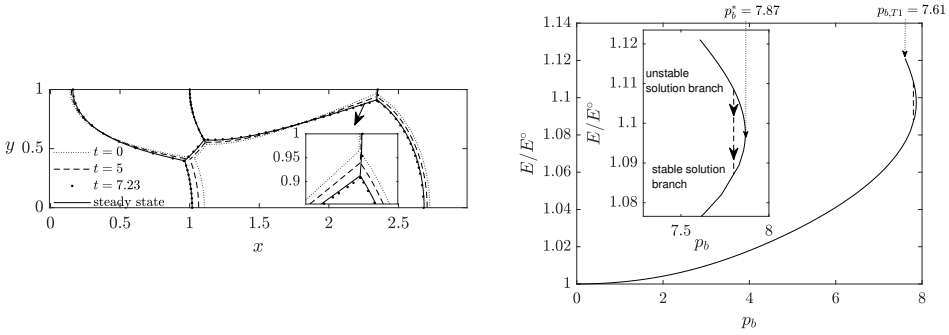

(a) (b)

Figure 5: (a) Film configurations obtained for a system set up in equilibrium with $l_1^\circ = 0.5$ and $l_2^\circ/l_1^\circ = 0.41$. The dotted line (the initial condition) corresponds to a steadily migrating shape on the second solution branch (with $p_b = 7.801 \leq p_b^* \approx 7.87$). The solid line corresponds to the system's steadily migrating shape on its first solution branch (with $p_b = 7.8 \leq p_b^* \approx 7.87$). In both cases the system is moving as a result of almost the same imposed back pressure. If we now set $p_b = 7.8$ and perform an unsteady simulation, then over time, the system on the second branch migrates away from the initial state. After a time $t \approx 7.23$ it is considered to reach a new steady state (which coincides with the first solution branch given by the solid line). (b) System energy for the steady state solution vs imposed back pressure. Here we can see the two solution branches connecting at a saddle-node bifurcation point. The first branch connects the equilibrium state to the saddle-node bifurcation, and a second branch connects the saddle-node bifurcation to a $T1_u$ topological transformation. On this second branch, p_b decreases from p_b^* to $p_{b,T1}$.

On the other hand, if the system is perturbed differently, it can migrate from a steady solution to a $T1$. This was observed to happen when either steady solution branch at $p_b = p_b^* - \delta p_b$, was used as an initial condition (assuming some small δp_b), and the system was perturbed dynamically by imposing $p_b = p_b^* + \delta p_b$ (a domain in which neither steady solution branch exists any longer). This then leads to a $T1$ (see section S 6(c)iii in the supplementary material).

To summarize when multiple steady states are present, it is possible to use unsteady state simulations to show the system migrating from one steady solution to another, both solutions having however the same topology. Steady state solutions need not exist however for all values of p_b. Instead any given steady solution branch typically terminates at some finite p_b^*. Outside the domain in which steady state solutions exist, the system is liable to break up via topological transformations, and this situation is considered next.

(c) Time and distance up to first topological transformation

As mentioned in section 2(e) (see also section S 2 in supplementary material), the three-bubble system was shown by [34] to undergo different types of topological transformations, provided large enough pressure p_b was imposed, and depending on the values of l_1° and l_2°/l_1°, i.e. depending on the bubble area distribution. However, the steady state findings of [34] contemplate a different physical situation from what we consider in this study: here, starting from equilibrium, we suddenly impose a specified p_b then hold it fixed over time, up to the system reaching a steadily migrating structure or undergoing a topological transformation. In the event that a $T1$ is reached, questions of time and distance to reach it now become relevant.

For small imposed back pressures we expect no $T1$, with the unsteady state system propagating instead for an arbitrarily long time, and eventually approaching a steadily migrating shape, typically the same shape as found by [34] via a steady state computation. In contrast, for sufficiently high p_b, systems are expected to undergo a $T1$ after a finite amount of elapsed time. The distance travelled to $T1$ meanwhile, is measured as the difference between the average horizontal coordinate location of films across the channels at the time of the topological transformation, compared to their location in the initial equilibrium structure. In this section we compute the time elapsed and the distance travelled up to the first topological transformation being reached for systems with $l_1^\circ = [0.1, 0.5, 0.9, 0.96]$ and in each case for values of $l_2^\circ/l_1^\circ = [0.1, 0.5, 0.9]$ at equilibrium.

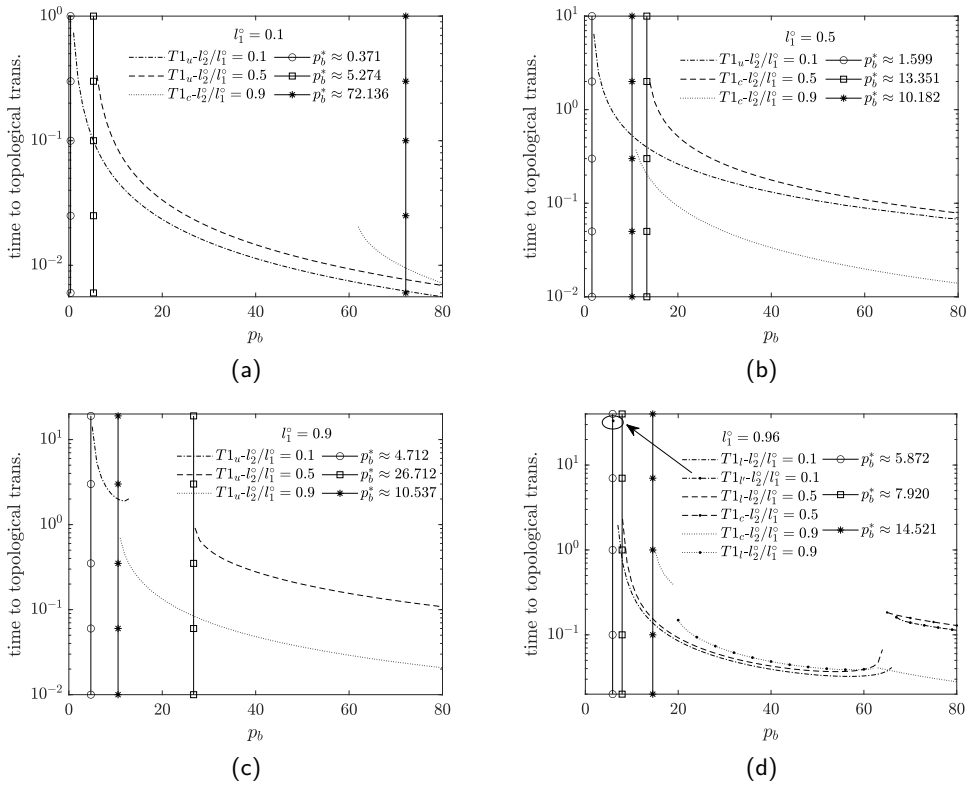

Figure 6: Time to topological transformation, obtained for different systems, which have in equilibrium (a) $l_1^\circ = 0.1$, (b) $l_1^\circ = 0.5$, (c) $l_1^\circ = 0.9$ and (d) $l_1^\circ = 0.96$. On the pressure axis, the back pressure p_b varies from 0 to 80 in steps of an integer. Note the logarithmic axis for time. We cannot typically find topological transformation to the left of the vertical lines, since steady state solutions exist in this domain: the p_b values labelling each of these vertical lines are the steady state predictions for p_b^*. Note in (c), that the first data set (dash-dotted line) stops at $p_b \approx 13$ and does not continue to higher p_b, i.e. the system ceases to break when $p_b \geq 13$. Instead, a new steady state not studied in [34], is found. Note also in (d), that one of the states is highlighted with an arrow because it is otherwise easy to overlook, given it occurs over only a very small p_b domain.

In Figure 6 we can see that as the imposed back pressure increases, the time elapsed up to the first topological transformation typically decreases. In Figure 7 we see a similar phenomenon for distance to the first topological transformation. Yet another observation we make comparing Figures 6 and 7 is that the variation in time to $T1$ with varying p_b (note the logarithmic axis for time) tends to be more significant than the variation in distance to $T1$. This is because long times to $T1$ tend to

correlate with low p_b, hence low propagation velocities. Short times to $T1$ meanwhile correlate with high p_b, hence high propagation velocities. Distance of course is the integral of velocity over time.

In both cases (Figures 6 and 7), as the imposed back pressure approaches the vertical lines, which correspond to the steady state critical pressures p_b^*, the time and distance travelled tend to diverge. This happens since steady state solutions without $T1$ were proven to exist in [34] for pressures lower than critical p_b^*. In at least one case however, as can be seen in Figure 6(a) for $l_1^\circ = 0.1$ and $l_2^\circ/l_1^\circ = 0.9$, we found unsteady state topological transformation for pressures smaller than the predicted critical pressure $p_b^* \approx 72.14$ (as obtained from a steady state solution in [34]). Specifically topological transformations happened for any p_b value greater than $p_b^{**} \approx 62$. We explore this situation further in section S 6(b) in supplementary material. It appears that in this situation, despite steady state solutions existing, the dynamic solution takes the system far away from any steady branches, which is why the system breaks.

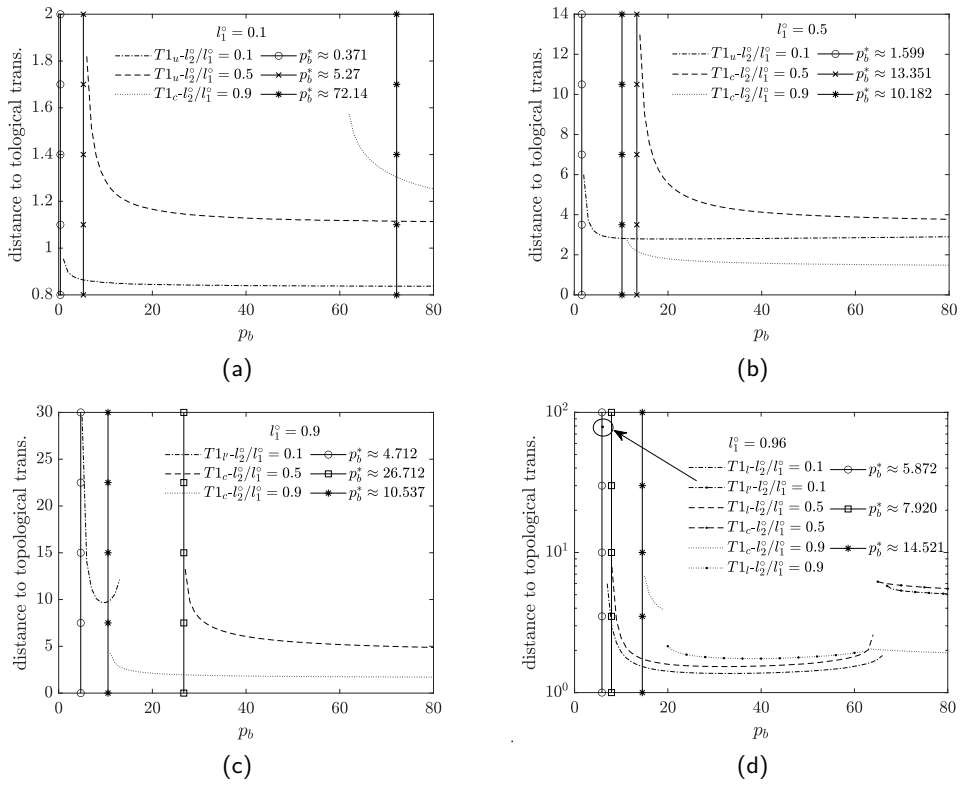

Figure 7: Distance travelled by the structure up to topological transformations, obtained for different systems, which have in equilibrium (a) $l_1 = 0.3$, (b) $l_1 = 0.5$, (c) $l_1 = 0.9$ and (d) $l_1 = 0.96$. On the pressure axis, the back pressure p_b varies from 0 to 80 steps of an integer. We cannot typically find topological transformation to the left side of the vertical lines, since steady state solutions exist in this domain.

(i) Different topological transformations for different back pressures

Another observation, as can be seen in Figure 6(d), is that different topological transformations can be reached for different imposed back pressures. For instance at $l_1^\circ = 0.96$ and $l_2^\circ/l_1^\circ = 0.1$ we see $T1_{l'}$ as the first transformation that occurs at $p_b = 6$ (only observed case), but this gives way to $T1_l$ for $p_b > 6$, and at even higher p_b values to $T1_l$ again. For the same l_1° but $l_2^\circ/l_1^\circ = 0.5$, $T1_l$ gives

way to $T1_c$ as p_b increases. Yet again at the same l_1° but $l_2^\circ/l_1^\circ = 0.9$, we see a switch from $T1_c$ to $T1_l$ and back again as p_b changes. Switches in the $T1$ type with varying p_b will be discussed further in section 4(d) and also in section S 6(d) in supplementary material. As seen in Figures 6(d) and 7(d), they are often associated with sharp changes in the time and distance to $T1$.

(ii) System that stops undergoing topological transformation at higher pressures

In the case of $l_1^\circ = 0.9$ and $l_2^\circ/l_1^\circ = 0.1$ (see Figure 6(c) and also Figure 7(c)), as back pressures higher than $p_b > 13$ are imposed, the system stops undergoing topological transformation. For this particular system, the steady state solution predicted no steady states to the right of the p_b^* vertical line. However the approach of [34] only tracked a steady solution branch starting from the equilibrium state plus any second branch to which that first one eventually connects. Additional branches of steady solutions might well exist, disconnected from these ones, and Figures 6(c) and 7(c) are evidently finding such a branch. This is further discussed in section S 6(a) in the supplementary material.

(iii) Physical implications of varying p_b and $T1$ type

The findings of Figures 6 and 7 have a number of physical implications. We have found that distance to topological transformation is typically a slowly decreasing function of driving pressure. Therefore, if it is desired to drive a foam structure intact through a real channel of a certain length, the data in the Figures 6 and 7, define a maximum permitted driving pressure, and hence a minimum time for driving the structure through the channel. On the other hand, one of the features we observe in Figures 6(d) and 7(d), is that in certain cases, the type of topological transformation can change at a certain p_b, sometimes leading to sharp changes in time and distance to $T1$. For instance in Figures 6(d) and 7(d), with $l_1^\circ = 0.96$ and $l_2^\circ/l_1^\circ = 0.9$, to allow the system to propagate more distance without breaking, we can set p_b so as to avoid the transition from $T1_c$ to $T1_l$ that happens around $p_b \approx 20$.

In addition, also in Figures 6(d) and 7(d) the $T1_l$ to $T1_c$ transition (for $l_1^\circ = 0.96$ and $l_2^\circ/l_1^\circ = 0.5$) and the $T1_l$ to $T1_{l'}$ transition for (for $l_1^\circ = 0.96$ and $l_2^\circ/l_1^\circ = 0.1$) both happening for p_b a little above 60 are desirable: the structure can migrate both further and faster without breaking. Although not seen in Figure 6 and Figure 7, another relatively common transition turns out to be between $T1_u$ at lower back pressure and $T1_c$ at higher back pressure. This is discussed in section S 6(d) in supplementary material and in particular in Figure S 8. There tends to be a slight increase in distance to $T1$ if we select pressure p_b just slightly above that transition. Compared to some of the cases shown in Figure 7(d) however, the relative change in distance to $T1$ as p_b varies in the case of Figure S 8 is actually rather modest. To summarize, since the topological transformation type can affect how far and how fast the structure can move along the channel, understanding how the transformation type changes is relevant to the design of processes involving transport along channels.

A final comment we make in this section, is that analysis of time and distance to topological transformation can be done not only for a three-bubble system but also for a simple lens. In this fashion we can compare and contrast the respective tendency to break up of the three-bubble system and the simple lens. This is done in section S 6(f) of supplementary material. What we find is that the three-bubble system can sometimes break up more easily than the simple lens (on the grounds that it is susceptible to modes of break up unavailable to the simple lens). On the other hand, the three-bubble system can sometimes be much harder to break than the simple lens, which results from the three-bubble system sometimes admitting states (unavailable to the simple lens) that avoid break up altogether. Which case (the three-bubble system or the simple lens) is easier or more difficult to break ultimately turns out to depend on bubble sizes.

(d) First topological transformation type as a function of p_b

As we have discussed, provided the three-bubble system undergoes topological transformation, the first transformation that it exhibits (see section 2(e)) can be one of five distinct types, denoted as $T1_c$, $T1_u$, $T1_{u'}$ (although this is very rare [34], and not actually observed in any of the cases studied in this work), $T1_{l'}$ and $T1_l$. Which of these transformations turns out to be the first to occur depends

on the size of the bubbles, which is set by fixing l_1° and l_2° at equilibrium. However, for specified l_1° and l_2°, we have now seen that which topological transformation is selected first can also potentially depend on the particular back pressure p_b that is imposed (for additional details on this, see e.g. supplementary material section S 7). Therefore, here we study at different imposed back pressures p_b the topological transformation behaviour of systems with different values of $l_1^\circ \in [0.1, 0.2, ..., 0.9, 0.96]$ and $l_2^\circ/l_1^\circ \in [0.1, 0.2, ..., 0.9]$.

This is what we show in Figure 8 expressed in the form of phase diagrams. Specifically phase diagrams in l_1° vs l_2°/l_1° are shown for a selection of p_b values $p_b \in [10, 20, 40, 80]$. There are of course (at least) two ways to produce phase diagrams such as these. One is the unsteady state simulation approach that we use here (applying the back pressure suddenly). The other is the steady state approach of [34] (increasing the back pressure gradually), relevant data for which are presented in section S 4. As [34] explains, in the steady state case, a contour plot shown in section S 4(b) can be consulted to decide if any topological transformation has taken place for a specified p_b, and if it has, the type of $T1$ can be obtained from a diagram in section S 4(a). Any discrepancies between the unsteady state and steady state approaches are indicated in Figure 8 by using "|" between the two predictions.

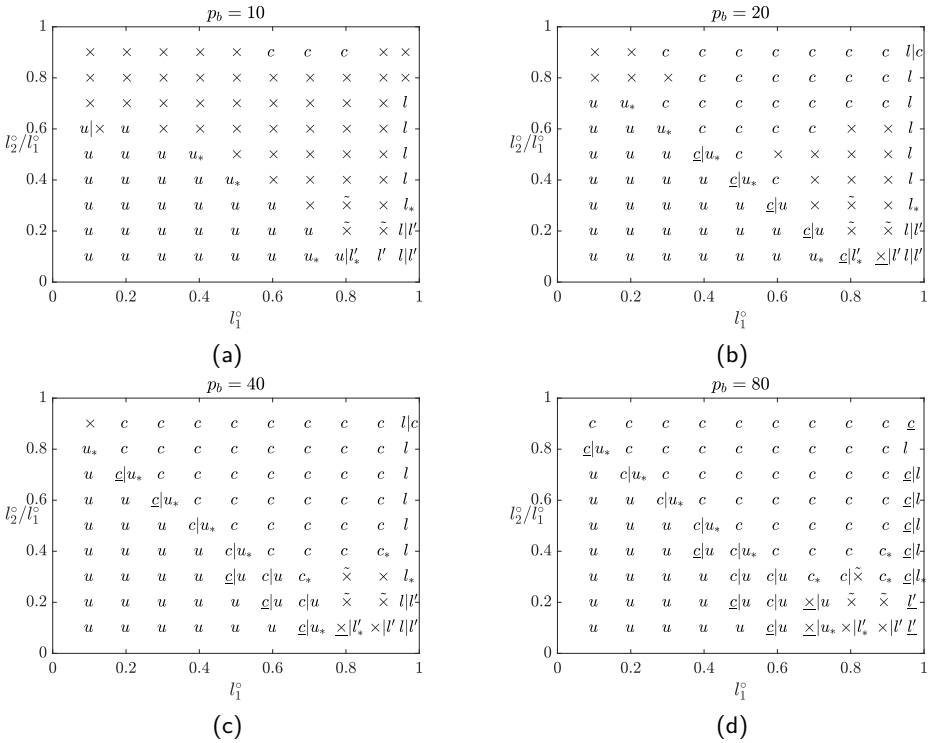

Figure 8: First topological transformation vs imposed back pressure p_b for (a) $p_b = 10$, (b) $p_b = 20$, (c) $p_b = 40$ and (d) $p_b = 80$. Here the first $T1$-type for each combination of l_1° and l_2° is denoted with its corresponding symbol c, u, l and l'. Both unsteady state and steady state predictions are contemplated. Cases in which the unsteady state methodology predicts a different situation from the steady state solution are specified side by side separated with "|" with the unsteady case shown first. If the steady state predictions involve $T1$s on second solution branches following saddle-node bifurcations, these are further specified by the subscript "$*$". Cases with no $T1$ (at least not yet at the p_b in question), but where a $T1$ is predicted eventually are labelled with $\times$. Cases where a $T1$ is never predicted (at least via the steady state approach) are labelled with $\tilde{\times}$. Cases in which the $T1$ type in the unsteady case differs from the type at the next pressure down are underlined.

(i) Differences between unsteady and state predictions

There are relatively few cases in which the unsteady state and steady state predictions differ in Figure 8. For the most part, any differences occur in regions of the phase diagram in which distinct transformation types are known to compete. For instance, based on the steady state results in Figure S 2(a) (in the supplementary material) there is competition between $T1_u$ and $T1_c$ down the diagonal of the phase diagram, competition between $T1_l$ and $T1_c$ towards the right hand boundary, and competition between many different $T1$ types in the bottom right hand corner (see the zoomed view in Figure S 2(b)).

Further to this and as was found by [34], different $T1$ types in a steady state phase diagram such as Figure S 2 are often separated by buffer regions (see also section 2(e)), in which saddle-node bifurcations are predicted (see section 4(b) and also S 3). In Figure 8 we add a subscript "$*$" if the steady state prediction corresponds to a saddle-node state. In such cases, the $T1$s that are predicted via the steady state analysis are typically on unstable solution branches (again see section 4(b)), so might not be easily reached via a dynamic simulation approach. This then is what Figure 8 finds: differences between unsteady state and steady state predictions are often associated with steady states of saddle-node type.

(ii) Effect of increasing p_b upon tendency for $T1$

From Figure 8(a)–(b) we can see that in many cases for p_b values as low as $p_b = 10$, there is no topological transformation (such cases are denoted with "$\times$") but as p_b increases to $p_b = 20$, systems tend to undergo $T1$, very often a $T1_c$. For $p_b = 40$ or $p_b = 80$ in Figure 8(c)–(d) there are only a few cases which have not undergone topological transformation, and they mostly correspond to moderately large l_1° with small to moderate l_2°/l_1°. The systems that have not undergone topological transformation are the ones that can achieve a geometrically invariant structure as studied in [34] (see also section S 4 in supplementary material).

Note that in Figure 8 we make a distinction between "$\times$" states (which have not undergone a topological transformation up to the given p_b) and "$\tilde{\times}$" states (which according to the steady state analysis of [34] would never undergo $T1$). Clearly there are only few $\tilde{\times}$ states, but the data do seem to suggest resisting transformation via the steady state analysis also ensures that transformation is resisted in an unsteady state situation. One exception is $l_1^\circ = 0.8$, $l_2^\circ/l_1^\circ = 0.3$ which is predicted to break via $T1_c$ at unsteady state when $p_b = 80$ for instance. One of the issues with the unsteady state simulation is that, owing to discretization, it cannot predict film lengths shorter than a specified minimum (see section 3(b)), and hence cannot approach any steady states which happen to have exceedingly short films. Nevertheless in this particular case, the steady state solution predicts film lengths to be sufficiently long for the unsteady solution to resolve.

Numerical discrepancies due to discretization are seen however elsewhere in the phase diagram, e.g. at $l_1^\circ = 0.1$ and $l_2^\circ/l_1^\circ = 0.6$ and $p_b = 10$. The unsteady state result predicts a $T1_u$, even though the steady state does not, but this is due to the steady state having a film shorter than the minimum length that the unsteady numerical method (see section 3(b)) would permit. Further discussion of such situations is given in section S 6(b) and also S 7 in supplementary material).

(iii) Effect of p_b upon type of $T1$

As well as affecting the tendency of systems to undergo $T1$, imposing different p_b values can also change $T1$ type. This is actually only an issue for unsteady state simulations, since the steady state case implies gradual increases in pressure p_b being imposed and the system always breaks once a critical value p_b^* is reached, and the pressure is not then raised any further. In the unsteady case however, the pressure p_b is imposed suddenly, and it is possible to select a pressure well above the pressure p_b^{**} needed to break a system. Differences in $T1$ type with respect to the next lower pressure in Figure 8 are specified by an underline, provided of course that the next lower pressure did actually undergo $T1$.

These underlined cases tend to be situations in which competition between different $T1$s is occurring. For instance along the diagonal in Figure 8(b)–(d) (at various different p_b) we see instances in which competition between $T1_u$ and $T1_c$ occurs. The steady state predicts $T1_u$ but the unsteady state (underlined cases) has just switched from $T1_u$ to $T1_c$. Likewise along the right hand boundary of the phase diagram (the data correspond to $l_1^\circ = 0.96$), there is competition between $T1_l$ and $T1_c$, with the steady state predicting $T1_l$ but the unsteady state switching from $T1_l$ to $T1_c$ for high enough p_b (underlined cases in Figure 8(d)). Looking at Figure 8(d) overall, it is clear that $T1_c$ is a common transformation type at the highest pressure $p_b = 80$ considered here. The above described cases concern situations in which increasing p_b creates a difference in predictions between steady and unsteady state approaches. However increasing p_b can also eliminate such difference. Lower down on the right hand boundary of the phase diagram for instance, there is competition between $T1_l$ and $T1_{l'}$. The steady state prediction is $T1_{l'}$ but the unsteady state prediction only switches from $T1_l$ to $T1_{l'}$ at high enough p_b (underlined cases in the bottom right of Figure 8(d)).

(iv) Eliminating topological transformation at high p_b

Although for the most part in Figure 8 increasing p_b causes $T1$s to happen, there are some cases in which the opposite occurs. For instance $l_1^\circ = 0.7$ and $l_2^\circ/l_1^\circ = 0.1$ does undergo topological transformation for $p_b \in [10, 20, 40]$ in Figure 8(a)–(c) (specifically $T1_u$ for $p_b \in [10, 20]$ and $T1_c$ for $p_b = 40$), whereas in Figure 8(d) for $p_b = 80$, no transformation occurs. Cases like this are marked with an underline "$\underline{\times}$" in Figure 8(b)–(d) (specifically they are indicated in this fashion for the pressure at which the transformation is found to be eliminated compared to the next pressure down). These states tend to be close by to the aforementioned $\tilde{\times}$ states (see section 4(d)ii), towards the bottom right hand corner of the phase diagram. These $\underline{\times}$ states are predicted to break if driven with a gradually increasing pressure, and likewise break if they are driven suddenly with a moderate pressure, but not break at all if they are driven suddenly with a very large pressure. How such a situation can come about is discussed further in section S 6(a) in the supplementary material. It is clear though that what determines the ultimate fate of the system, is not just the back pressure that is eventually imposed, but the manner in which it is imposed.

To summarize regardless of whether an unsteady state or steady state methodology is employed, the main trend we see as back pressure p_b is increased is that more and more systems undergo topological transformation. In the unsteady state case however switching between different types of $T1$ states as p_b changes is also possible. Via both steady state solution and unsteady state simulation, we have found certain systems that do not undergo any topological transformation even for large imposed back pressure. As shown in Figure 8, these cases do not always match up between unsteady state and steady state prediction, although even so, they are still reasonably close together in the phase diagram in terms of their l_1° and l_2°/l_1° values. In these particular cases, whether or not topological transformation occurs may depend on whether the pressure is slowly increased from the equilibrium (quasistatically, i.e. finding steady states for each pressure) or is suddenly imposed (dynamic simulation).

There is therefore a considerable amount of information in Figure 8 (and furthermore some of this information is captured in a statistical fashion in supplementary material section S 6(e)). However it is worth remembering that this figure shows only the first topological transformation. After the first topological transformation, additional $T1$s may occur. The various sequences of transformations that result and the configurations to which they lead, remain as open questions.

5. Conclusions

We have computed unsteady state simulations for a three-bubble system, which corresponds to a truncated version of the infinite staircase structure. Many different sets of bubble areas have been considered, by setting different values of l_1° and l_2°, which correspond at equilibrium to the vertical distances from the upper channel wall to vertices V_1 (equivalently V_3) and V_2, respectively.

Moving away from equilibrium, we have determined the evolution over time of systems as they migrate through a confined straight channel, looking at a range of imposed back pressures p_b to drive the flow. The unsteady state approach used here (sudden imposition of the back pressure) differs from the steady state approach of [34] (gradual increase of the back pressure).

Steady state solution revealed [34] that for certain combinations of l_1° and l_2° different solution branches could exist meeting at a saddle-node bifurcation. The present work however has demonstrated that not all these solution branches are stable. However those steady solution branches that joined up with the equilibrium state were stable, so in principle are physically achievable. A three-bubble system can thereby remain intact as it is driven along a channel under increasing imposed pressure, as long as the steady solution branch exists. If the system is driven under too high a back pressure however, the branch may come to an end, and the structure typically breaks up via a topological transformation. What appears moreover to be key to driving topological transformation here is asymmetry. Since we have an odd number of bubbles, there are unequal numbers of films on different sides of the channel, and hence (with viscous drag tied to the films) unequal drag on different sides.

Via the steady state approach, various types of topological transformations e.g. $T1_c$ (vertex-vertex collision), $T1_u$ (transformation at the upper channel wall) and $T1_l$ or $T1_{l'}$ (transformation at the lower channel wall) were identified in [34]. Meanwhile via unsteady state simulation as performed here, the same types of topological transformations were found, albeit not always under identical conditions as we describe below.

(a) First topological transformation

In the present work, we focussed just on the first topological transformation that occurred. The first topological transformation in the unsteady state system often (but not always) onsets at an imposed back pressure comparable with the pressure at which it occurs in the steady state approach. Moreover the type of transformation ($T1_c$, $T1_u$, $T1_l$, $T1_{l'}$) at onset often (but again not always) matched the type of transformation seen in the steady state system. Exceptions occurred for combinations of l_1° and l_2° (i.e. for certain choices of bubble areas) at which competition between different transformation types was present. Systems with those sets of bubble areas then evolve in a fashion that is sensitive to the history of how the driving pressure is imposed.

Another observation is that even though at the pressure of onset, there is a reasonable match between the $T1$ type from steady state solution and unsteady state simulation, if a driving pressure far above onset is used, this no longer applies. Indeed the $T1_c$ (vertex-vertex collision) becomes the most common $T1$ type (at least for the first topological transformation) as p_b is increased. Interestingly the $T1_c$ also seemed to be particularly common for long trains of bubbles [1] (at least when those trains move in an asymmetric U-bend as per [1]). Understanding how the $T1_c$ occurs at different driving pressures in three-bubble systems might then be relevant for understanding the behaviour of long trains of bubbles.

Knowing how the topological transformation type changes with changing p_b is potentially relevant for delivering bubble structures at high speed through long but finite channels: at any given driving pressure, break up can be avoided provided channel length remains less than the distance required to achieve topological transformation. For systems that break up via a specified topological transformation type, time elapsed and distance travelled up to $T1$ were shown to be decreasing functions of driving pressure, and thereby decreasing functions of propagation speed. However when a driving pressure was reached at which the topological transformation changed from one type to another, sharp changes in time elapsed and distance travelled up to $T1$ were sometimes observed. By selecting driving pressure on the appropriate side of these sharp changes, it is possible that a structure might be driven much further and possibly even much faster along channels, and still arrive at the end of the channel without yet breaking up.

We have also compared (see supplementary material section S 6(f) for details) the time and distance to break up for the three-bubble system with the time and distance to break up for the simple lens (a single bubble plus an additional film). Despite the fact that a system with a very large

number of bubbles (an infinite staircase) is known to resist $T1$, in the systems studied here, the addition of bubbles (in particular going from the simple lens to the three-bubble system) does not necessarily imply longer time and distance to break up. This is because the three-bubble system is susceptible to modes of break up that are unavailable to the simple lens. However there are certain parameter regimes (i.e. certain combinations of l_1° and l_2° or equivalently certain bubble areas) in which the three-bubble system (albeit not the simple lens), manages to avoid break up altogether (at least according to steady state calculations of [34]). In such regimes, the system achieves instead a geometrically invariant state, in which bubbles reach a fixed shape, but merely propagate faster and faster as driving pressure increases. Close by to these regimes then, the time and distance to break the three-bubble system can turn out to exceed the time and distance to break the simple lens.

(b) Situations avoiding topological break up

We found instances in which the steady state computations for the three-bubble system predicted no break up even at arbitrarily large driving pressures, but the unsteady state simulations led to topological break up even so. Once again the history of how driving pressure is imposed (whether as a gradual increase or as a sudden imposition) is seen to affect the system. On the other hand we also found the converse, i.e. a sudden imposition of a large driving pressure enabling the system to avoid topological transformation even though a gradual pressure increase would drive a topology change.

This behaviour has been found to be associated (see supplementary material section S 6(a)) with the existence of a steady state solution branch which connected with the geometrically invariant state (corresponding to the limit of arbitrarily high imposed pressure) but which was disconnected from the equilibrium state (corresponding to zero imposed pressure, and joining up with a solution branch that terminated at comparatively modest pressure). The existence of a solution branch at "high pressure" means that for a suitably chosen history of imposed pressures it might be possible to drive certain three-bubble systems into the geometrically invariant state, such that bubbles can be delivered intact arbitrarily far along channels arbitrarily fast.

In [34] a necessary condition for the existence of the geometrically invariant state was identified, and a large domain of l_1° and l_2° values satisfied that condition. In the work of [34] however, very few of the systems satisfying the necessary condition actually attained the geometrically invariant state, and the reasons were unclear. Based on the present work however, it appears that gradual increases in pressure (the strategy of [34]) may not always be the best way to attain the geometrically invariant state and the rapid transport of bubbles along channels that it admits. Instead the sudden imposition of a large pressure may actually be a better way to realize rapid transport.

Of interest of course is what happens when more bubbles are added to the system. Adding more than three bubbles is likely to make it easier for a system to achieve a geometrically invariant state, given that in an infinite staircase, bubbles can in principle move at arbitrarily large velocities, without deformation. It is unclear however how the number of bubbles in a train will affect the likelihood that the geometrically invariant state will be on a solution branch that connects up with equilibrium, as opposed to on a solution branch that is disconnected from equilibrium. Which situation is the case will dictate how driving pressures need to be applied over time (either gradually or suddenly) in order to move many bubbles quickly along channels without break up.

Finally we note that in cases when topological transformations cannot be avoided, the present work has only considered the first topological transformation that systems encounter. In reality though systems are likely to undergo a sequence of topological transformations, and the unsteady state simulation methodology utilised here is capable of studying this. Multiple topological transformations and the transformation paths that systems take will be addressed in future work.

Ethics. This research raises no ethical issues.

Data Accessibility. All results presented here are reproducible by mathematical results and/or mathematical procedures detailed in the article and the supplementary material or else via numerical algorithms (accessible via https://strathcloud.sharefile.eu/d-s6a6ecaf051ea4927bbad091b29cf2475), which are also detailed in the article and the supplementary material.

Authors' Contributions. C. T.-U. performed mathematical analysis, developed computer code, ran computations, analysed data, prepared the first draft of the article and reviewed and edited subsequent drafts. P. G. conceived the study, provided supervision, performed mathematical analysis, analysed data and reviewed and edited article drafts. Both authors approved the final version and agree to be accountable for all aspects of the work.

Competing Interests. We declare we have no competing interests.

Funding. C. T.-U. and P. G. acknowledge funding from EPSRC grant EP/V002937/1.

Acknowledgements. C. T.-U. acknowledges S. Cox and D. Vitasari for hosting a short research visit during which useful discussions took place.

References

1. Drenckhan W, Cox SJ, Delaney G, Holste H, Weaire D, Kern N. 2005 Rheology of ordered foams: On the way to discrete microfluidics. Colloids and Surf. A: Physicochem. and Eng. Aspects **263**, 52–64. doi: 10.1016/j.colsurfa.2005.01.005.
2. Atencia J, Beebe DJ. 2005 Controlled microfluidic interfaces. Nature **437**, 648–55. doi: 10.1038/nature04163.
3. Stevenson P. 2012 Foam engineering: Fundamentals and applications. Chichester: John Wiley & Sons.
4. Shan D, Rossen WR. 2004 Optimal injection strategies for foam IOR. SPE J. **9**, 132–150. doi: 10.2118/88811-PA.
5. Wang S, Mulligan CN. 2004 An evaluation of surfactant foam technology in remediation of contaminated soil. Chemosphere **57**, 1079–1089. doi: 10.1016/j.chemosphere.2004.08.019.
6. Jia X, Mowatt G, Burr JM, Cassar K, Cook J, Fraser C. 2007 Systematic review of foam sclerotherapy for varicose veins. Br. J. Surg. **94**, 925–936. doi: 10.1002/bjs.5891.
7. Géraud B, Jones SA, Cantat I, Dollet B, Méheust Y. 2016 The flow of a foam in a two-dimensional porous medium. Water Resour. Res. **52**, 773–790. doi: 10.1002/2015WR017936.
8. Shen X, Zhao L, Ding Y, Liu B, Zeng H, Zhong L, Li X. 2011 Foam, a promising vehicle to deliver nanoparticles for vadose zone remediation. Journal Hazard. Mater. **186**, 1773–1780. doi: 10.1016/j.jhazmat.2010.12.071.
9. Zhong L, Szecsody JE, Zhang F, Mattigod SV. 2010 Foam delivery of amendments for vadose zone remediation: propagation performance in unsaturated sediments. Vadose Zone J. **9**, 757–767. doi: 10.2136/vzj2010.0007.
10. Eneotu M, Grassia P. 2020 Modelling foam improved oil recovery: Towards a formulation of pressure-driven growth with flow reversal. Proc. Roy. Soc. A **476**, 20200573. doi: 10.1098/rspa.2020.0573.
11. Kern N, Weaire D, Martin A, Hutzler S, Cox SJ. 2004 Two-dimensional viscous froth model for foam dynamics. Phys. Rev. E **70**, 041411. doi: 10.1103/PhysRevE.70.041411.
12. Höhler R, Cohen-Addad S. 2005 Rheology of liquid foam. J. Phys. Condens. Matter **17**, R1041–R1069. doi: 10.1088/0953-8984/17/41/R01.
13. Cox S, Weaire D, Glazier JA. 2004 The rheology of two-dimensional foams. Rheol. Acta **43**, 442–448. doi: 10.1007/s00397-004-0378-3.
14. Green TE, Bramley A, Lue L, Grassia P. 2006 Viscous froth lens. Phys. Rev. E **74**, 051403. doi: 10.1103/PhysRevE.74.051403.
15. Cox SJ, Weaire D, Mishuris G. 2009 The viscous froth model: Steady states and the high-velocity limit. Proc. Roy. Soc. A **465**, 2391–2405. doi: 10.1098/rspa.2009.0057.
16. Okuzono T, Kawasaki K. 1995 Intermittent flow behavior of random foams: A computer experiment on foam rheology. Phys. Rev. E **51**, 1246–1253. doi: 10.1103/PhysRevE.51.1246.
17. Kim D, Seol Y, Kim Y. 2021 Numerical study on rheology of two-dimensional dry foam. Phys. Fluids **33**, 052111. doi: 10.1063/5.0050010.
18. Durian DJ. 1995 Foam mechanics at the bubble scale. Phys. Rev. Lett. **75**, 4780–4783. doi: 10.1103/PhysRevLett.75.4780.
19. Durian DJ. 1997 Bubble-scale model of foam mechanics: Melting, nonlinear behavior, and avalanches. Phys. Rev. E **55**, 1739–1751. doi: 10.1103/PhysRevE.55.1739.
20. Drenckhan W, Hutzler S. 2015 Structure and energy of liquid foams. Adv. Colloid Interface Sci. **224**, 1–16. doi: 10.1016/j.cis.2015.05.004.

21. Grassia P, Montes-Atenas G, Lue L, Green TE. 2008 A foam film propagating in a confined geometry: Analysis via the viscous froth model. Eur. Phys. J. E **25**, 39–49. doi: 10.1140/epje/i2007-10262-8.
22. Vitasari D, Cox S. 2017 A viscous froth model adapted to wet foams. Colloids and Surf. A: Physicochem. and Eng. Aspects **534**, 8–15. doi: 10.1016/j.colsurfa.2017.04.064.
23. Vitasari D, Cox S, Grassia P, Rosario R. 2020 Effect of surfactant redistribution on the flow and stability of foam films. Proc. Roy. Soc. A **476**, 20190637. doi: 10.1098/rspa.2019.0637.
24. Cantat I, Kern N, Delannay R. 2004 Dissipation in foam flowing through narrow channels. Europhys. Lett. **65**, 726–732. doi: 10.1209/epl/i2003-10169-0.
25. Spencer MA, Jabeen Z, Lubensky DK. 2017 Vertex stability and topological transitions in vertex models of foams and epithelia. Eur. Phys. J. E **40**, 1–17. doi: 10.1140/epje/i2017-11489-4.
26. Stewart PS, Davis SH. 2012 Dynamics and stability of metallic foams: Network modeling. J. Rheol. **56**, 543–574. doi: 10.1122/1.3695029.
27. Jiang Y. 1996 Extended large-Q Potts model simulation of foam drainage. Philos. Mag. Lett. **74**, 119–128. doi: 10.1080/095008396180489.
28. Weaire D, Kermode JP. 1984 Computer simulation of a two-dimensional soap froth II. Analysis of results. Philos. Mag. B **50**, 379–395. doi: 10.1080/13642818408238863.
29. Durand M, Stone HA. 2006 Relaxation time of the topological $T1$ process in a two-dimensional foam. Phys. Rev. Lett. **97**, 226101. doi: 10.1103/PhysRevLett.97.226101.
30. Okuzono T, Kawasaki K, Nagai T. 1993 Rheology of random foams. J. Rheol. **37**, 571–586. doi: 10.1122/1.550383.
31. Reinelt DA, Kraynik AM. 2000 Simple shearing flow of dry soap films with tetrahedrally close packed structure. J. Rheol. **44**, 453–471. doi: 10.1122/1.551096.
32. Gopal AD, Durian DJ. 1995 Nonlinear bubble dynamics in a slowly driven foam. Phys. Rev. Lett. **75**, 2610–2613. doi: 10.1103/PhysRevLett.75.2610.
33. Cox S. 2005 A viscous froth model for dry foams in the Surface Evolver. Colloids and Surf. A: Physicochem. and Eng. Aspects **263**, 81–89. doi: 10.1016/j.colsurfa.2004.12.061.
34. Torres-Ulloa C, Grassia P. 2022 Viscous froth model applied to the motion of two-dimensional bubbles in a channel: The three-bubble case. Proc. Roy. Soc. A **478**, 20210801. doi: 10.1098/rspa.2021.0642.
35. Hutzler S, Weaire D, Cox SJ, van der Net A, Janiaud E. 2007 Pre-empting Plateau: The nature of topological transitions in foam. Europhys. Lett. **77**, 28002. doi: 10.1209/0295-5075/77/28002.
36. Reinelt DA, Kraynik AM. 1993 Large elastic deformations of three-dimensional foams and highly concentrated emulsions. J. Colloid Interface Sci. **159**, 460–470. doi: 10.1006/jcis.1993.1347.
37. Press WH, Teukolsky SA, Vetterling WT, Flannery BP. 1988 Numerical recipes in C. Cambridge: Cambridge University Press.